5

STATE OF THE SCIENCE REGARDING RF DOSIMETRY, MEASUREMENT, AND CERTIFICATION

Om P. Gandhi

Introduction

Cellular telephones and wireless personal communication systems (PCS) are being introduced into society at a very rapid rate. Whereas the present-day cellular telephones in the United States operate at midband transmission frequencies of about 835 MHz (about 900 MHz in Europe), higher frequencies on the order of 1900 MHz (1800 MHz in Europe) are to be used for the PCS systems, including mobile telephones, wireless local area networks, pagers, personal health monitoring systems, global positioning systems, etc. This has resulted in public concern about the health hazards of radiofrequency (RF) electromagnetic fields that are emitted by these devices. To allay public concerns, the Federal Communications Commission (FCC) in the United States has decided to require compliance with the ANSI/IEEE RF safety guidelines (American National Standards Institute/Institute of Electrical and Electronics Engineers [ANSI/IEEE], 1992) for uncontrolled environments for all personal wireless devices that use more than 100 mW of time-averaged input power to the antenna. According to ANSI/IEEE safety guidelines for uncontrolled environments (ANSI/IEEE, 1992), the mass-normalized rate of electromagnetic energy absorption (specific absorption rate or SAR) in any 1 gram of tissue should not exceed 1.6 W/kg except for the hands, wrists, feet, and ankles where the spatial-peak SAR shall not exceed 4 W/kg, as averaged over any 10 grams of tissue. The safety guidelines being proposed for the European Union are more lax and peak SARs of 2.0 W/kg for any 10 grams of tissue are considered acceptable for exposures of the general public (European Committee for Electrotechnical Standardization [CENELEC], 1995) for tissues other than hands, wrists, feet, and ankles, where the safety guidelines are similar to those of ANSI/IEEE (ANSI/IEEE, 1992).

In this paper we present a review of the numerical as well as experimental methods that may be used not only for compliance testing but also for design of cellular telephones and other PCS devices that minimize energy absorbed in the body

and maximize radiated energy. It is clear that increasingly accurate models, both numerical and experimental, and calculation and measurement procedures will be needed as the wireless revolution progresses to the use of higher and higher frequencies for a myriad of present and future applications. We will also outline some of the challenges in this area, particularly for applications at the higher microwave frequencies.

Numerical Methods

Analytical and numerical methods have been developed over the last 40 years to understand coupling of electromagnetic fields to biological bodies (Lin & Gandhi, 1995). While the earliest of the models involved homogeneous and layered planar, spherical, cylindrical, prolate spheroidal, and ellipsoidal models, the focus in the last 20 years has been on development of increasingly sophisticated, anatomically-based models that are capable of providing information on induced current and SAR distributions from a variety of far-field and near-field sources from extremely low frequencies (ELF) to microwave frequencies (Gandhi, 1990, 1995). These models have been shown to be capable of predicting the frequencies and polarization conditions of highest absorption by the human body (the so-called resonant conditions) and the likely high SARs in the human legs for vertically polarized incident fields in the VHF range—results that have led to frequency-dependent safety standards and the more recent inclusion of the induced current limits in the various safety guidelines (ANSI/IEEE, 1992; CENELEC, 1995).

Several numerical methods such as the method of moments (MOM), multiple multipole method, volume-surface integral equation method, finite integration technique (FIT), finite-element time-domain method, and finite-difference time-domain method (FD-TD), etc., have been developed for calculation of SAR distributions (Gandhi, 1990; Lin & Gandhi, 1995; Simunic, 1995). As evidenced from the published literature (Dimbylow & Mann, 1994; Gandhi & Chen, 1995; Gandhi, Chen, & Wu, 1994; Jensen & Rahmat-Samii, 1995) and the proceedings of a recent COST 244 meeting (Simunic, 1995), a method of choice for calculations of SAR distributions for coupled near-field devices such as cellular telephones is the FD-TD method. This method is perhaps the most popular of the numerical electromagnetic methods at the present time and has been used for a myriad of other electromagnetic problems as well, such as RF microwave antennas and circuit design, radar scattering from objects of various types, and issues of electromagnetic compatibility and interference (Kunz & Luebbers, 1993; Taflove, 1995).

A major advantage of this method is that the computer memory requirement and the computation time increase linearly as the number of voxels (volume pixels) into which an interaction space of interest, including the cellular telephone and the coupled parts of the body, (e.g., the models of the head and the hand) can be divided. This is a considerable improvement over N^2 and N^3 for some of the methods, such as MOM. Highly discretized volumes with N on the order of 10^6-10^7, and with cell sizes on the order of 1-3 mm, can, therefore, be used to obtain SAR distributions for anatomically realistic models. The perceived advantages of the FD-TD method over other numerical

techniques for mobile telephone dosimetry are given in the following.

1. It is considerably more efficient than traditional numerical electromagnetic methods such as the MOM, allowing use of realistic, anatomically-based models with resolutions on the order of 1-3 mm, using readily available computing workstations.

2. Since electrical properties such as the dielectric constants and conductivities of various tissues are not known with a high degree of precision, and accurate knowledge of these properties is evolving at the present time, it is relatively simple to incorporate these for dosimetric calculations using the numerical procedures.

3. It is also simple to alter the voxel sizes to calculate SAR distributions for heads of various sizes representative, for example, of women and children, and to use various postures of the telephones vis-à-vis the body.

4. Even though simple parallelepiped metal boxes covered with plastic have, to date, been used to model the handsets, the FD-TD procedure is perfectly capable of reading data files of software such as AutoCAD and Pro Engineer defining the exact geometry of the handset and its contents, albeit with a resolution of 1-3 mm, that is possible with the memories of today's readily available computing workstations. It has been alleged that this resolution may be inadequate to properly model the RF currents that may flow on internal substructures of the new transceivers, resulting in inaccurate SAR distributions. Our experience, however, has been that the microwave parts of the circuit are enclosed in a shielding metal box which in recent devices may only be a fraction of the handset. This can certainly be modeled in the FD-TD method.

5. Lastly, numerical procedures such as the FD-TD method permit calculations of the radiation patterns for a conceived wireless device coupled to the human body permitting, therefore, design of these devices that give desirable radiation patterns and lowest SARs that are within the safety guidelines.

Measurement Methods

Simple and more complex experimental models (phantoms) have and are being developed to obtain SAR distributions for actual operating wireless devices (Balzano, Garay, & Steel , 1978; Balzano, Garay, & Manning, 1995; Chatterjee, Gu, & Gandhi, 1985; Chou, personal communication, 1994; Cleveland & Athey, 1989; Gabriel, personal communication, 1994; Gandhi & Chen, 1995; Gandhi et al., 1994; Guy & Chou, 1986; Kuster & Balzano, 1992; Schmid, Egger, & Kuster, 1996; Stuchly, Spiegel, Stuchly, & Kraszewski, 1986). For the simplest of these models, homogeneous tissue-simulating gels or fluids are used in some sort of an insulating

container which gives the phantom the shape of the body that is to be modeled (Balzano et al., 1978, 1995; Chatterjee et al., 1985; Guy & Chou, 1986; Schmid et al., 1996). For the more complex experimental models, several different tissue-simulant compositions representing the important regions such as the skin, skull, eyes, brain, etc. are used (C.K. Chou, personal communication, 1994; Cleveland & Athey, 1989; C. Gabriel, personal communication, 1994; Gandhi & Chen, 1995; Stuchly et al., 1986). In liquid or semi-solid forms, it is quite cumbersome to keep these materials of different compositions from mixing with each other to create more homogeneous properties. Procedures such as surrounding these materials with thin plastic wraps or other separators are therefore used. Since the human anatomy is quite complex, such phantoms consisting generally of two to four or five tissue types do not necessarily match the anatomical details of the head or any other region that is to be modeled. Some authors have, therefore, focused on using homogeneous tissue-simulating fluids and on realistic exposure conditions (actual handsets, spectacle frames, etc.). Fluids rather than gels are preferred to facilitate rapid movement of the internal E-field sensor which is driven by a stepper motor or a robot for determination of the 3-D SAR distribution from which 1- or 10-gram peak SARs can be obtained for compliance with the safety guidelines.

The resolution of the measurements is on the order of several millimeters because of the E-field sensor dimensions that are typically on the order of 4–5 mm (Balzano et al., 1995; Bassen & Babij, 1990; Bassen & Smith, 1983; Schmid et al., 1996). Since the amount of tissue-simulant material that is displaced by these sensors is quite significant (on the order of $\lambda_e/4$ in wet tissues at the PCS frequencies on the order of 1.8-2.2 GHz), this is likely to influence the field distribution that one is trying to measure, particularly at the higher frequencies. Smaller E-field sensors would therefore be needed for dosimetry at higher wireless communication frequencies.

The FD-TD Method

The FD-TD method has been described in several publications (Dimbylow & Mann, 1994; Gandhi, 1990, 1995; Gandhi & Chen, 1995; Gandhi et al., 1994; Jensen & Rahmat-Samii, 1995; Lin & Gandhi, 1995; Simunic, 1995) and a couple of recent textbooks (Kunz & Luebbers, 1993; Taflove, 1995). In addition to many applications in the various areas of microwave design and calculations (Kunz & Luebbers, 1993; Taflove, 1995), this method has also been used successfully to obtain SARs for anatomically based models of the human body for whole-body or partial-body exposures to spatially uniform or nonuniform (far-field or near-field) electromagnetic fields from ELF to microwave frequencies (Gandhi, 1990, 1995; Lin & Gandhi, 1995). In this method, the coupled Maxwell's equations in differential form are solved for all points of the absorber (model of the human head and neck and the approximate model of the hand), as well as the space including the plastic-covered handset, the antenna embedded in a dielectric sheathing and the region to the absorbing boundaries which are generally taken to be at least 10 cells away from the telephone-head/neck coupled region (Dimbylow & Mann, 1994; Gandhi & Chen, 1995; Gandhi et al., 1994; Jensen & Rahmat-Samii, 1995). Various absorbing boundary conditions such as Mur's

second-order boundary condition (Mur, 1981), retarding-time boundary condition (Berntsen & Hornsleth, 1994), and, more recently, Berenger's perfectly matched layer boundary condition (Berenger, 1994) have been used by the various authors. Negligible differences in the calculated SAR distributions or the radiation patterns are obtained regardless of the boundary conditions that are used (Cui, Chen, & Gandhi, 1995).

Even though the FD-TD method has been thoroughly tested against analytical solutions, measured data, and other numerical techniques for far-field exposures, it has not, until recently, been subjected to such rigorous validation for near-field exposures. We have recently started to focus on this issue. In the following section we give some near-field test cases where excellent agreement is found between the results obtained using the FD-TD method and other analytical and/or other procedures (Furse & Gandhi, 1995).

Validation Test Runs

Dipole Antenna Near a Two-Layered Half-Space

The first validation was for a dipole antenna very near a layered half-space. The geometry is shown in Figure 1. An exact, analytical solution, based on expansion of the fields from the dipole and enforcement of the boundary conditions at the planar surfaces, is given in King (1993). For the specific case given, the frequency is 900 MHz, the dipole is of length l = 12 cm, and is located at a distance d_o = 2 cm away from the first layer. The first layer is 1-cm-thick skull-equivalent material, with ε_r = 5.977 and σ = 0.09913 S/m. The second layer is infinitely thick brain-equivalent material with ε_r = 50.2852 and σ = 1.3423 S/m.

For the FD-TD method, a cell size of 5 mm is used in the horizontal (x, y) directions, and 9.23 mm in the vertical (z) direction. This gives an antenna 13 cells long, with the feedpoint in the center cell, and a distance of 4 cells between the antenna and the first layer, which is 2 cells thick. The second layer is supposed to be infinitely thick, which is modeled by a thickness of 24.5 cm (49 cells), which is sufficiently thick to attenuate all of the fields to well below 1 percent of their peak values before the end of the material is reached. The infinite nature of the two-layered half-space in the x- and z-directions was modeled by considering a sufficiently large box so that the fields were very small at the edges. This box is taken to be 12 cm (24 cells) in the x-direction and 33.3 cm (36 cells) in the z-direction. The simulation was run for 10 cycles, but convergence was observed at about eight cycles.

Figure 2 shows the magnitude of the electric field along the y-axis, comparing the analytical solution (see Table 1 of King, 1993) with the values calculated by the FD-TD method. Values are normalized to a feedpoint current of 100 mA rms.

A similar test geometry is given in Figure 10 of Kuster and Balzano (1992). This simulation is made at 840 MHz, with a half-wave dipole antenna located 1.5 cm from the first layer, which is 1-cm-thick bone-equivalent material, having properties ε_r = 5, σ= 0.15 S/m. The second layer is brain with properties ε_r = 42, σ = 0.75 S/m. The

FD-TD simulation is run with a horizontal cell size of 5 mm and vertical cell size of 5.9655 mm. The infinite absorbing material is modeled as before, using a large box of dimensions x = 12 cm, y = 30 cm (including both layers), and z = 39.4 cm. The simulation is run for 10 cycles.

Figure 3 shows the SAR values along the y-axis comparing the MMP method of Kuster and Balzano (1992) and the FD-TD results. Values are normalized to a feedpoint current of 100 mA rms. The close agreement of FD-TD solutions to the analytical and MMP solutions for a dipole antenna in front of an infinite layered space give good confidence in FD-TD's ability to correctly model antennas in close proximity to an absorbing material. The following simulation analyzes the effect of a finite-sized model on the FD-TD solution.

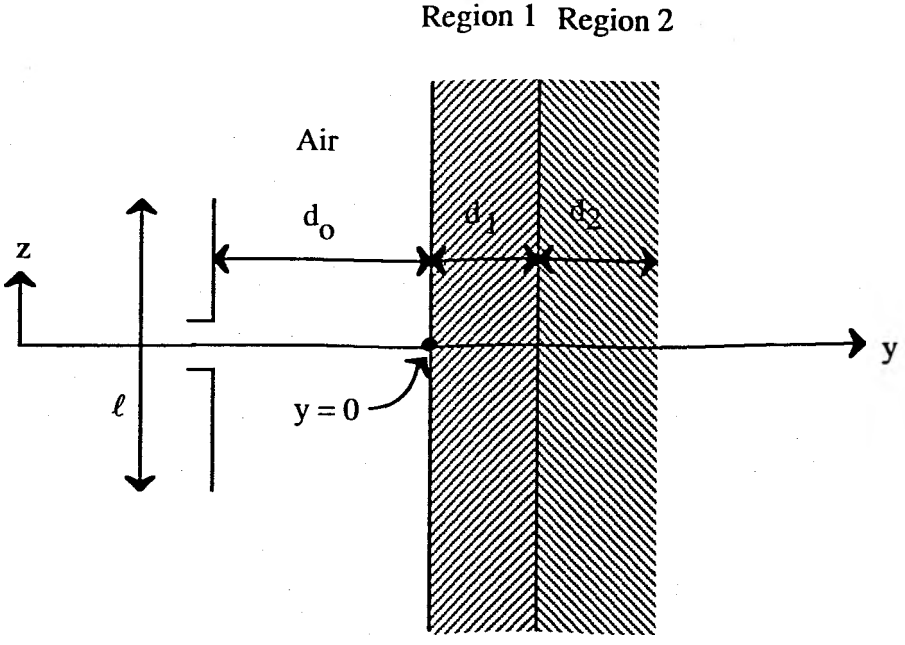

Figure 1. A dipole antenna in front of a layered half-space. For the test case in King (1993), the frequency is 900 MHz, ℓ = 12 cm, d_0 = 2 cm, d_1 = 1 cm, d_2 = ∞ (24.5 cm), ε_{r1} = 5.977, σ = 0.09913, ε_{r2} = 50.2852, σ_2 = 1.3423. The FD-TD simulation uses $\Delta x = \Delta y$ = 5 mm, Δz = 9.23 mm.

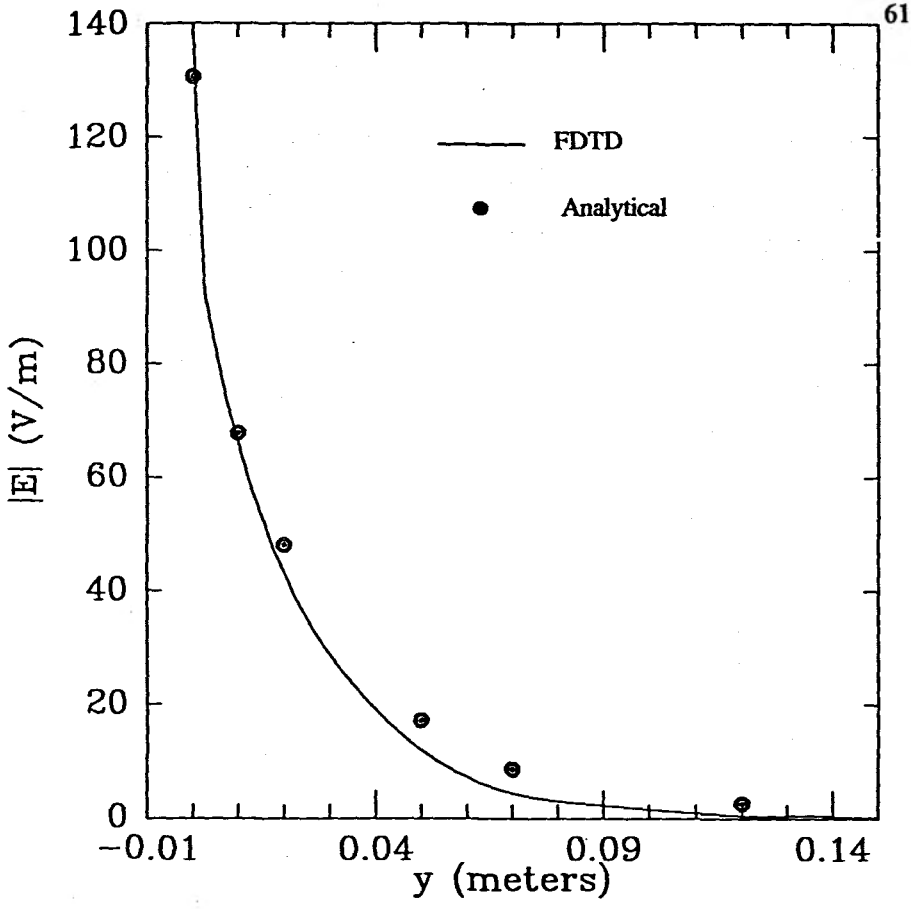

Figure 2. Magnitude of the electric field along the y axis for the model shown in Figure 1. Values are compareed for the FD-TD simulation and analytical data from King (1993).

A Dipole Antenna Near an Absorbing Box of Finite Dimensions

The second validation was for a dipole antenna near an absorbing box of finite dimensions. This was similar to the first validation, except that the finite nature of the box was accurately modeled, and measured data was available (see Figure 3 of Kuster & Balzano, 1992) for comparison. The frequency was 840 MHz, and the dipole was 17.3 cm long. It was located a distance d_o from the box, with the feedpoint centered in front of the box, which was $15 \times 30 \times 50$ cm^3 in the x, y, z directions, respectively.

The box was made of 5-mm-thick acrylic glass (assumed to be polystyrene with ε_r=2.55). Since the cell sizes used in this simulation were slightly larger than the thickness of the acrylic, an effective dielectric constant for the glass was calculated from the formula (Gandhi et al., 1994):

$$\varepsilon_{eff}^{-1} = \frac{\varepsilon_r \Delta}{\varepsilon_r(\Delta - W) + W}$$

where Δ is the size of the FD-TD cell, W is the thickness of the acrylic, and ε_r is the dielectric constant of this material. This formula is derived by finding the average fields at the air-dielectric interface and setting them equal to the fields in a larger-sized cell, giving the smaller effective dielectric constant given above. The box is filled with brain-simulating material with $\varepsilon_r = 53$ and $\sigma = 1.4$ S/m (Kuster & Balzano, 1992).

Figure 4 shows the SAR distributions along the y-axis comparing the FD-TD simulations and measurements made by Kuster and Balzano (1992) for various

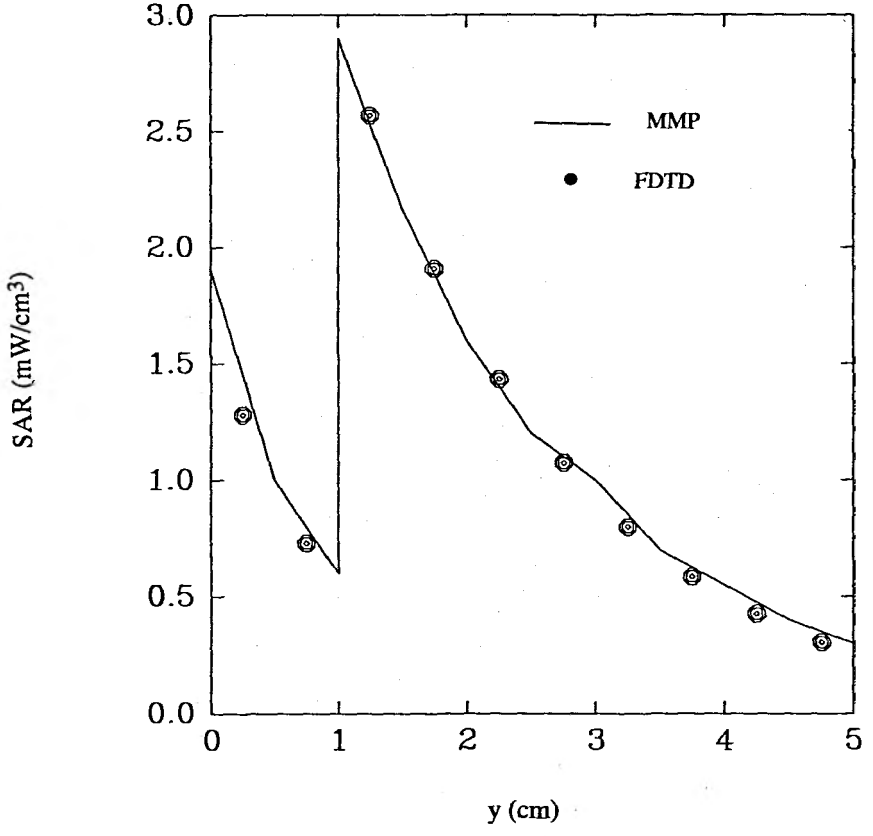

Figure 3. Magnitude of the electric field along the y-axis for the model shown in Figure 1 with a frequency of 900 MHz, $d_0 = 1.5$ cm, $d_1 = 1$ cm, $d_2 = \infty$ (39.4 cm), $\ell =$ 17.3 cm, $\varepsilon_{r1} = 5.0$, $\sigma_1 = 0.15$, $\varepsilon_{r2} = 42$, $\sigma_2 = 0.75$. The FD-TD simulation uses $\Delta x = \Delta y = 5$mm, $\Delta z = 5.9655$ mm. Values are compared with the MMP results of Kuster and Balzano (1992).

distances, d_o, between the dipole and the box. The FD-TD simulations use a cell size of $\Delta z = 5.9655$ mm, and $\Delta x = \Delta y = 5.133$, 5.1, 6.35, and 7.6 mm for the separation distances between the antenna and the box of $d_o = 15.4$, 20.4, 25.4, and 30.4 mm, respectively. The vertical cell size, Δz, was chosen to precisely model the height of the antenna, and the horizontal cell size, Δx, Δy, was chosen to precisely model the separation distance, d_o. Values which are used for ε_{eff} are 2.388, 2.426, 1.918, and 1.666 for the four different cells' sizes, respectively. Simulations are run for 2500 time steps, and convergence is observed at about 1500 time steps. Values are normalized to a feedpoint current of 100 mA rms.

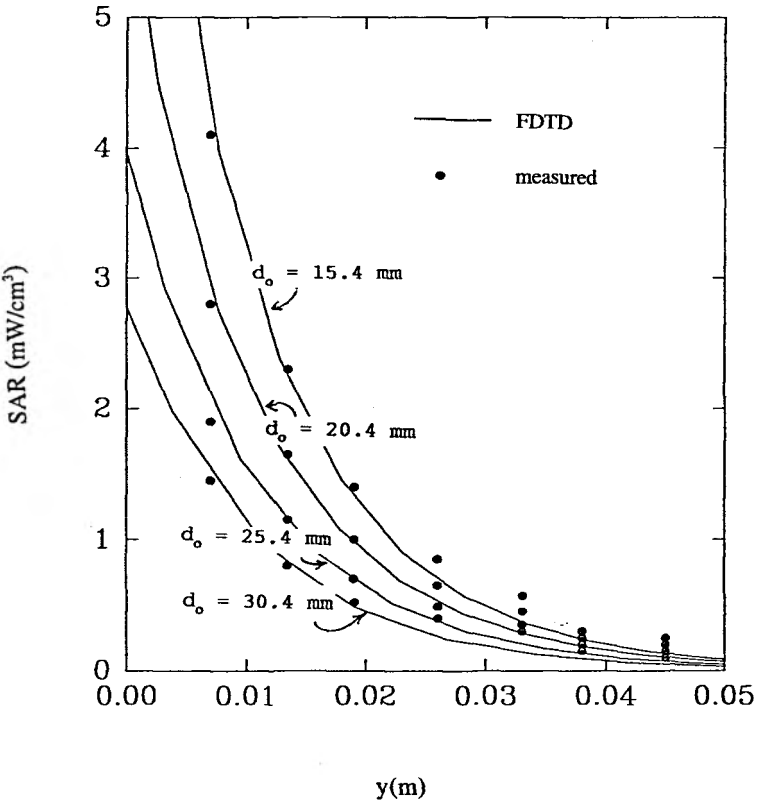

Figure 4. SAR distribution along the y-axis for the dipole antenna in front of the phantom box. Frequency = 840 MHz. Values are given for different separation distances, d_o, between the dipole and box, as compared with measured data from Kuster and Balzano (1992).

An Infinitesimal Dipole Near a Sphere

The test case simulations for cases 1 and 2 give good confidence in the FD-TD

method's ability to correctly predict the field or SAR distribution within a planar phantom as a function of distance between the antenna and phantom. These simulations do not require modeling of curved surfaces that are associated with the high-resolution head models in cellular phone studies. The test cases 3 and 4 demonstrate FD-TD's ability to correctly analyze fields within spherical objects that do require modeling of curved surfaces. For this FD-TD analysis, the curved object was modeled using "stair stepping," or cubical cells filling the curved object. Thus, the smaller the sphere relative to the cell size, the coarser the modeling approximation.

For this test case, an infinitesimal dipole is located 1.5 cm away from a 20-cm-diameter brain-equivalent sphere (Dhondt & Martens, 1994). The frequency is 900 MHz, and the properties taken for the sphere are $\varepsilon_r = 43$ and $\sigma = 0.83$ S/m. The infinitesimal dipole is modeled as a single feedpoint location, without the surrounding antenna from the previous test cases. The FD-TD cell size is $\Delta x = \Delta y = \Delta z = 5$ mm, which makes the sphere 40 cells in diameter.

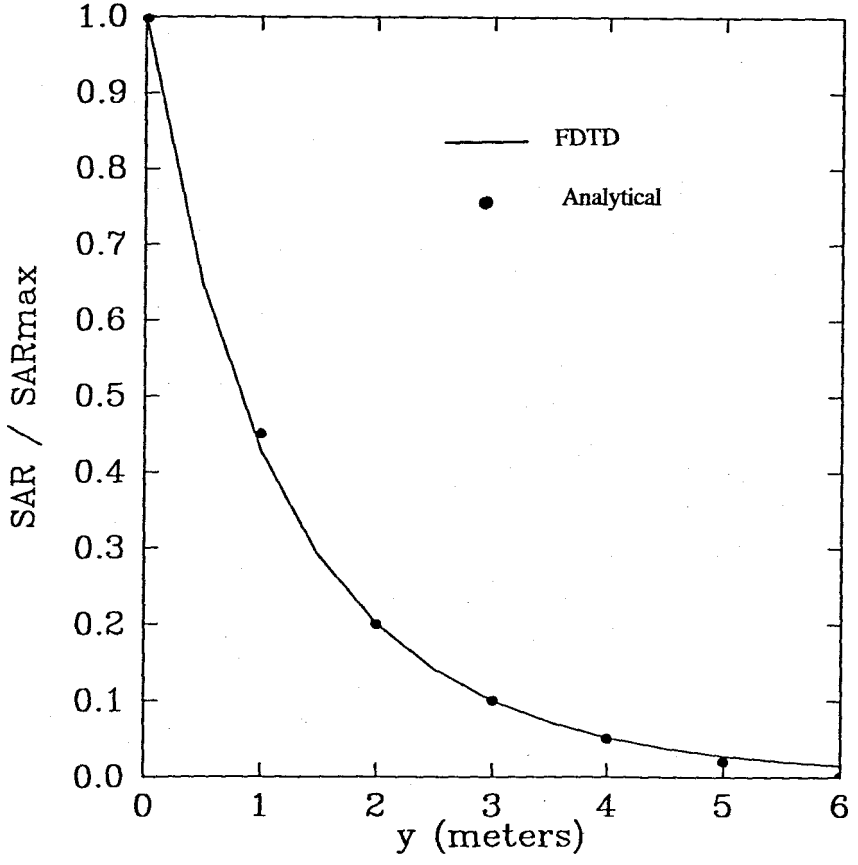

Figure 5. Relative SAR distribution along the y-axis of the homogeneous brain-equivalent sphere excited by an infinitesimal dipole. Analytical data is taken from Dhondt and Martens (1994).

Figure 5 shows the relative SAR along the y-axis from the front edge of the sphere calculated using the FD-TD method and compared to an analytical solution based on the Bessel function expansion (Dhondt & Martens, 1994). The excellent agreement here again adds confidence that the FD-TD method can accurately model curved absorbing models. The following simulation adds to that confidence by examining a full-sized antenna near a sphere, comparing not only the trend of the field distribution, but its absolute magnitude as well.

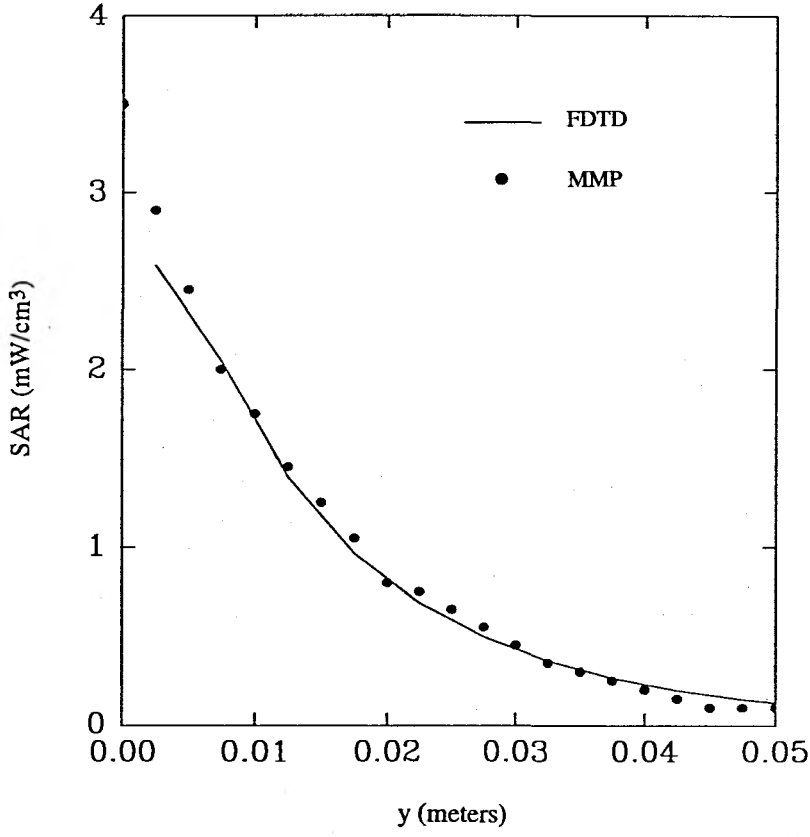

Figure 6. SAR distribution along the y-axis of the homogeneous brain-equivalent sphere excited by a 17.3 long dipole antenna. Values are compared with the MMP solution of Kuster and Balzano (1992). Diameter = 10 cm; frequency = 840 MHz.

A Dipole Antenna Near a Lossy Sphere

The next test case was for a dipole antenna near a homogeneous brain-equivalent sphere. The frequency is 840 MHz, and the approximately half-wave-long dipole antenna (l = 17.3 cm) is located 2.5 cm from the sphere. The sphere has a radius of 10

cm. This is modeled with an FD-TD cell size of $\Delta x = \Delta y = 5$ mm, and $\Delta z = 5.9655$ mm, and the simulation was run for 1500 time steps. The dielectric properties used for the sphere are $\varepsilon_r = 55$, $\sigma = 1.4$ S/m. Figure 6 shows the SAR distribution along the y-axis from the front edge of the sphere, for the two different sizes of the sphere. The FD-TD simulations are compared to MMP simulation data from Kuster and Balzano (1992). Once again, the excellent comparisons give confidence that FD-TD can accurately model antennas in the very near field of curved absorbing objects.

Anatomic Models of the Human Body

As aforementioned, heterogeneous anatomically-based models, particularly of the human head, are needed to obtain the SAR distributions due to mobile telephones. Based on magnetic resonance imaging (MRI) and/or computed tomography (CT) scans, millimeter-resolution anatomic models of the human body are becoming increasingly available and are being used for dosimetry of cellular telephones (Dimbylow & Mann, 1994; Gandhi, 1990, 1995; Gandhi & Chen, 1995; Gandhi et al., 1994; Jensen & Rahmat-Samii, 1995; Lin & Gandhi, 1995). Whereas a somewhat cruder model of the human head with a resolution of 6.56 mm was used in Jensen and Rahmat-Samii (1995), a higher-resolution MRI-based model with a 2-mm cell size has been used by Dimbylow and Mann (1994).

We have developed a millimeter-resolution model of the human body (Gandhi, 1995; Gandhi & Chen, 1995; Gandhi et al., 1994) from the MRI scans of a male volunteer of height 176.4 cm and weight 64 kg. The MRI scans were taken with a resolution of 3 mm along the height of the body and 1.875 mm for the orthogonal axes in the cross-sectional planes. Even though the height of the volunteer was quite appropriate for an average male, the weight was somewhat lower than an average of 71 kg, which is generally assumed for an average male. This problem can, to some extent, be ameliorated by assuming that the pixel dimensions for the cross sections are larger than 1.875 mm by the ratio of $(71/64)^{1/2} = 1.053$, (i.e., 1.974 mm instead of 1.875 mm). Using a software package from the Mayo Clinic called ANALYZE, the MRI scans of the human body were converted into images involving 30 tissue types whose electrical properties (ε_r, σ) can then be prescribed at the mobile telephone midband frequencies of 835 MHz or 1900 MHz. The 30 tissues taken for the whole-body model are: muscle, fat, regular bone, compact bone, cartilage, skin, nerve, intestine, spleen, pancreas, heart, blood, parotid gland, liver, kidney, lung, bladder, cerebrospinal fluid, eye humour, eye sclera, eye lens, stomach, erectile tissue, prostate gland, spermatic cord, testicle, ligament, brain, pineal gland, and pituitary gland. Since only the model of the head and neck is used for the present calculations, only 15 of these tissues are involved in this model. The theoretical weights of each of the major tissues were calculated based on specific gravities defined by the International Council on Radiation Protection and Measurements (International Council on Radiation Protection and Measurements [ICRP], 1992) and the number of voxels of each tissue in the model. These weights are given in Table 1 and are compared to the weights of the tissues of the average "reference" man (ICRP, 1992). Most of the comparisons are excellent. The reasons for some of the discrepancies between the reference man and model weights are given in the footnotes of Table 1.

Tissue Type	Mass Density g/cm^3	No. of Voxels	Weight in grams	
			Model	reference man (ICRP, 1992)
muscle	1.047	2,604,370	31,871	28,000
fat	0.916	1,388,947	14,873	13,500
bone[1]	1.465	564,906	9,675	10,000
cartilage	1.097	13,839	177[2]	2,500
skin[3]	0.983	289,720	3,329	2,600
nerve	1.038	5,410	65.6[4]	30[5]
intestine	1.042	104,204	1,270[9]	1,010[10]
pancreas	1.045	9,394	114.8	100
heart	1.030	59,236	713.1[9]	450[10]
blood	1.058	58,074	718[6]	5,500
liver	1.030[8]	146,074	1,759	1,800
kidney[7]	1.050	24,780	304	310
lung[7]	0.347	242,731	983.8	1,000
bladder	1.030	18,053	217.4[9]	150-250
stomach	1.05	47,914	588[9]	150[10]
prostate gland	1.045	2,830	34.5	16
testicle[7]	1.044	7,223	88.1	60
ligament	1.220	29,472	420	1,500
pineal gland	1.048	18	0.2	0.18
pituritary gland	1.066	22	0.3	0.6
brain	1.035	138,188	1,673	1,400

[1] Compact and regular bone combined. [2] Major cartilage regions (ear, nose) only. No bone-end cartilage. [3] 1-voxel thick layer around entire body except eyes and ear canal. [4] Spinal cord, optic nerve, other large nerves included. [5] Spinal cord only. [6] Major arteries and vessels only. [7] Pair. [8] No value given. Estimate based on tissue content. [9] Full (contents are not differentiated from organ). [10] Empty (organ only).

Table 1. Comparison of weights of tissues/organs in the MRI-based model with "reference man" (ICRP, 1992)

The new dielectric properties assumed for the various tissues at 835 and 1900 MHz are given in Table 2. These are taken from the unpublished data of C. Gabriel (personal communication, 1994). Also included at the bottom of Table 2 are the lower dielectric properties for fat, bone, and cartilage previously reported in the literature (Durney, Massoudi, & Iskander, 1986; Stuchly & Stuchly, 1980). We have considered two orientations of the handset, one that is held vertically relative to the head (tilt angle of 0°) and another that is held at a tilt angle of 30° relative to the head (see Figure 7). To simulate a handset that is typically tilted forward by 30° for a vertically erect head, we have modified the MRI-based model so that it is tilted forward by 30°. As described in Lazzi and Gandhi (1997), the forward tilt is accomplished by a "best fitting" technique wherein each of the cells of the present model is assigned to a new corresponding cell only if no other cells have a better fitting to the new one. An error matrix proportional to the distance of the rotated cells from the cell centroid of the new cell is used and minimized to obtain the original cells that may occupy the new cell location. The 30° forward-tilted head thus obtained is shown in Figure 7 together with the original untilted head model. For the tilted model, a vertical orientation of the handset and the antenna allows more accurate modeling of their shapes and dimensions. Models for each of the antennas and the handsets were assumed to be covered with insulating materials of ε_r=4.0. Because of the different cell sizes used, particularly for the smaller models representative of 10- and 5-year-old children, different values of ε_{eff} obtained from Equation 1 have been used for the various simulations for these cases.

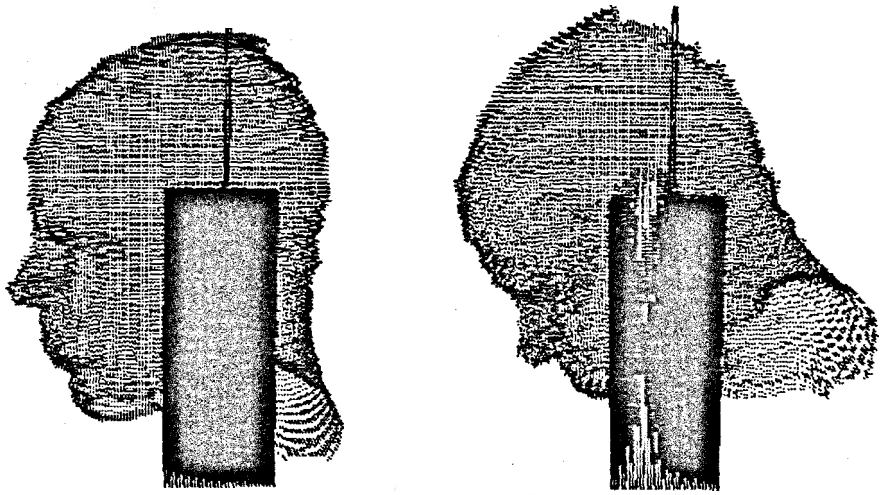

a. vertical b. tilted 30° relative to vertical

Figure 7. The two head models with the telephone used for the calculations.

Tissue	Spec. Gravity 10^3kg/m^3	835 MHz ε_r	835 MHz σ S/m	1900 MHz ε_r	1900 MHz σ S/m
muscle	1.04	51.76	1.11	49.41	1.64
fat	0.92	9.99	0.17	9.38	0.26
bone (skull)	1.81	17.40	0.25	16.40	0.45
cartilage	1.10	40.69	0.82	38.10	1.28
skin	1.01	35.40	0.63	37.21	1.25
nerve	1.04	33.40	0.60	32.05	0.90
blood	1.06	55.50	1.86	54.20	2.27
parotid gland	1.05	45.25	0.92	43.22	1.29
CSF	1.01	78.10	1.97	77.30	2.55
eye humour	1.01	67.90	1.68	67.15	2.14
sclera	1.17	54.90	1.17	52.56	1.73
lens	1.10	36.59	0.51	42.02	1.15
pineal gland	1.05	45.26	0.92	43.22	1.29
pituitary gland	1.07	45.26	0.92	43.22	1.29
brain	1.04	45.26	0.92	43.22	1.29
		Old properties (Durney et al., 1986; Stuchly & Stuchly, 1980)		Old properties (Durney et al., 1986; Stuchly & Stuchly, 1980)	
fat	0.92	7.20	0.16	9.70	0.27
bone (skull)	1.81	7.20	0.16	8.40	0.15
cartilage	1.10	7.20	0.16	9.70	0.27

Table 2. Dielectric properties and specific gravities of the various tissues assumed at the midband mobile telephone frequencies of 835 and 1900 MHz (Gabriel, 1996). Also included are the lower dielectric properties for fat, bone, and cartilage previously reported in the literature (Durney, Massoudi, & Iskander, 1986; Stuchly & Stuchly, 1980).

Because of the proximity of the hand to the telephone, it is essential to also model the hand for numerical calculations. For calculations to date we have modeled the hand by a region of 2/3 muscle-equivalent material of thickness 1.974 cm (10 δ_y) wrapped around the handset on three sides, with the exception of the side facing the head, with height two-thirds that of the handset.

By scaling the cell sizes of the MRI-based model, we have developed smaller models of the head, neck, and hand to correspond to dimensions characteristic of 10- and 5-year-old children, respectively. In the Dosimetry Handbook (Durney et al., 1986), the heights and weights for average 10- and 5-year-old children are given as 1.38 and 1.12 m and 32.5 and 19.5 kg, respectively. These heights and weights are also in agreement with the averages for the boys given in Lentner (1984). To obtain models of these needed heights, we have scaled the cell size $\delta_z = 3$ mm of the MRI-based model of the adult male of height 176.4 cm to new dimensions $\delta_z = 2.3469$ and 1.9048 mm, respectively. Also, maintaining the square shapes of the pixels in the cross-sectional planes as for the MRI-based model, we have altered the dimensions $\delta_x = \delta_y$ from 1.875 mm of the adult male model of weight 64.0 kg to new cell sizes $\delta_x = \delta_y = 1.51$ and 1.2989 mm to obtain models of 10- and 5-year-old children of weights 32.5 and 19.5 kg, respectively. The approximate hand dimensions have been similarly scaled through these cell sizes so that the hands cover less than two-thirds of the heights of the assumed handsets for models of 10- and 5-year-old children.

It is well-known that considerably lower values of ε_r and σ have previously been reported for fat, bone, and cartilage in the published literature (Durney et al., 1986; Stuchly & Stuchly, 1980) as compared to the higher values that have recently been determined by C. Gabriel (1996). These lower values of ε and σ reported for fat, bone, and cartilage, given at the bottom of Table 1, have been taken instead of the newer values for some of the runs (see Table 6) to determine the effect of tissue properties on SAR distributions.

We are aware of a preprint of a paper that has recently been submitted for publication (Hombach, Meier, Burkhardt, Tay, & Kuster, 1996). As referred to in the companion article by Kuster (1998), three different anatomically based models, two of these with a resolution as low as 1 mm, have been used for dosimetric calculations (Hombach et al., 1996) using the FIT implemented in the commercially available package MAFIA (CST, 1994). As given by the authors, "the lower part of the head was assigned to only one tissue type." The more serious problems for this paper pertain to the elimination of the ear in these models "to avoid increased effects caused by different ear modeling" and use of dipole antennas rather than the handset. It is well known that the highest SARs are obtained for the ear and the volumetric region of the tissues behind it. For all of the calculations given in this paper (see Tables 3 and 4, and also Dimbylow & Mann, 1994; Gandhi & Chen, 1995; Jensen & Rahmat-Samii, 1995), we have not only included the ear but assumed it to be squished against the head. Furthermore, the SAR distribution is sensitive to the exact modeling of the antenna, the handset, and the posture of the handset vis-à-vis the human head.

Even though models with resolution on the order of 1 mm are now becoming available, models with 2-3 mm resolution are quite adequate for frequencies of 1-2 GHz since it has previously been shown that FD-TD cell sizes as large as $\lambda_e/5$ are perfectly capable of giving accurate SAR distributions (Gandhi, Gu, Chen, & Bassen,

1992). For a frequency of 2 GHz, the wavelength λ_e in high-water tissues such as muscle, skin, and brain is about 23 mm and cell sizes on the order of 2-3 mm certainly observe the aforementioned requirement. It is recognized that finer-resolution models would indeed be needed for still higher-frequency wireless devices. Toward this end, we are presently developing the next-generation model of the human body with a resolution of 0.9375 mm along each of the three orthogonal axes.

	New properties	Old properties	Homogeneous model
Peak 1-voxel SAR (W/kg)	10.86	8.52	15.98
Peak 1-g SAR (W/kg)	2.93 (1.00g)	2.05 (1.00g)	4.17 (1.03 g)
Peak 1-g SAR for brain (W/kg)	1.13 (1.09 g)	0.86 (1.02 g)	—
Power absorbed by head and neck	45.0%	44.0%	41.5%
Power absorbed by "hand"	9.2%	11.9%	8.4%
Peak 1-voxel SAR for brain (W/kg)	1.62	2.11	—
CSF average (mW/kg)	72.7	62.6	—
Brain average (mW/kg)	72.3	62.9	—
Humour average (mW/kg)	31.8	32.9	—
Lens average (mW/kg)	11.3	12.8	—
Sclera average (mW/kg)	17.8	19.4	—

Table 3. SAR distributions for different properties of the various tissues. A $\lambda/4$ antenna above a handset is taken for the calculations at 835 MHz. Radiated power = 600 mW.

The Peak 1-Gram SAR

According to the ANSI/IEEE C95.1-1992 RF safety guideline for uncontrolled environments, the spatial-peak SAR should not exceed 1.6 W/kg for any 1 gram of tissue defined as a tissue volume in the shape of a cube (ANSI/IEEE, 1992). Because of the irregular shape of the body (e.g., the ears) and tissue heterogeneities, a tissue volume in the shape of a cube of, say, 1 × 1 × 1 cm will have a weight that may be in excess of, equal to, or less than 1 gram. Larger or smaller volumes in the shape of a cube may, therefore, need to be considered to obtain a weight of about 1 gram. Furthermore, for an anatomic model such as ours using unequal cell sizes (1.974 ×

	λ/4 antenna	3λ/8 antenna
Peak 1-voxel SAR (W/kg)	3.90	2.66
Peak 1-g SAR (W/kg)[1]	0.52 (1.01 g; 98.7%)	0.32 (1.01 g; 98.7%)
Peak 1-g SAR (W/kg)[2]	1.11 (1.03 g; 81.0%)	0.69 (1.06 g; 86.0%)
Peak 1-g SAR (W/kg)[3]	1.03 (1.10 g; 82.4%)	0.69 (1.11 g; 86.1%)
Peak 1-g SAR for brain (W/kg)[2]	02.0 (1.00 g)	0.16 (1.00 g)
Peak 1-g SAR for brain (W/kg)[3]	0.19 (1.05 g)	0.16 (1.00 g)
Power absorbed by head and neck	35.6%	29.4%
Power absorbed by "hand"	13.8%	7.0%
Peak 1-voxel SAR for brain (W/kg)	0.29	0.26
CSF average (mW/kg)	8.0	8.3
Brain average (mW/kg)	7.6	7.6
Humour average (mW/kg)	3.2	2.6
Lens average (mW/kg)	1.5	1.3
Sclera average (mW/kg)	1.8	1.5

[1] 5 x 5 x 3 cells; 0.987 x 0.987 x 0.9 cm; 0.88 cm^3
[2] 5 x 5 x 4 cells; 0.987 x 0.987 x 1.2 cm; 1.17 cm^3
[3] 6 x 6 x 3 cells; 1.184 x 1.184 x 0.9 cm; 1.26 cm^3
It was not possible to obtain 1-g weight of the brain for subvolume 1; hence., the 1-g SAR for brain for this case is not given.

Table 4. SAR distributions for the squished-ear model of the adult male for λ/4 and 3λ/8 antennas at 1900 MHz. Time-averaged radiated power = 125 mW.

1.974 × 3 mm), it is not very convenient to obtain exact cubical volumes even though nearly cubic shapes may be considered. We have, therefore, considered 5 × 5 × 3, 5 × 5 × 4, and 6 × 6 × 3 cells for the model of the adult male to obtain subvolumes on the order of 1 cm^3. For each of these subvolumes selected close to and around the regions of the high SARs, we have divided the absorbed powers by the weights calculated for the individual subvolumes to obtain 1-gram SARs. Furthermore, we have considered only those subvolumes where at least 80 percent of the cells are occupied by the tissues and no more than 20 percent of the cells are in air. As expected, there is a great deal of variability in the 1-gram SARs that are obtained. In keeping with the ANSI/IEEE safety guidelines, weights equal to or in excess of 1 gram are considered to obtain the

spatial-peak SARs that are given in Table 4 for two assumed lengths of monopole antennas above a metal box of dimensions 14 δ_x × 28 δ_y × 51 δ_z (2.76 × 5.53 × 15.3 cm) and 1-cell thickness δ of plastic covering of effective dielectric constant ε_{eff} given by Equation 1, which is somewhat lower than the dielectric constant ε_r of the actual insulation layer of thickness w (generally 1 mm).

In Table 4, it is interesting to note that even though the peak 1-gram SARs for the superficial tissues are highly variable (by almost 2:1), the corresponding values for the internal tissues, such as the brain, are nearly identical regardless of the subvolumes that are considered. The reason for the highly variable peak 1-gram SARs for the superficial tissues is that various subvolumes of, say, 0.8-1.2 cm^3 in the shape of a cube may each give a weight of about 1 gram, depending on the amount of air in such subvolumes. For our case, larger subvolumes such as 5 × 5 × 4 and 6 × 6 × 3 cells with volumes of 1.17 and 1.26 cm^3, respectively, involve more of air and the ear tissues and still have weights of at least 1 gram, whereas the smaller subvolumes of 5 × 5 × 3 cells with a total volume of 0.88 cm^3 must have more of the non-ear head tissues in order to get weights of 1 or more grams of weight. Since the subvolumes to consider for peak 1-gram SARs have not been clearly defined in the ANSI/IEEE safety guidelines (ANSI/IEEE, 1992), the variability in the peak 1-gram SARs given in Table 4 is hard to resolve and is clearly troublesome. All three peak 1-gram values have, therefore, been given in Table 4. For each of the cases, the weights and percentage of tissues by volume are given within parentheses of the peak 1-gram SARs.

This problem of lack of definition of the subvolume to consider was brought to the attention of the Dosimetry Working Group[2] of Wireless Technology Research (WTR), LLC. At its meeting in Duarte, California, on 30 October 1995, the working group decided to recommend to ANSI/IEEE that the tissue subvolume to consider should not extend beyond the most exterior surfaces of the body (e.g., the upper, lower, and side boundaries of the ear) but may include the air that is contained therein (e.g., the air in the crevices of the ear). Also, the weight of the subvolume may not be smaller than 1 gram, but preferably as close to it as possible. For the SAR data given in Table 4, this corresponds to case 2 with a peak 1-gram SAR of 1.11 W/kg for the $\lambda/4$ antenna and 0.69 W/kg for the 3 $\lambda/8$ monopole antenna above the handset.

Comparison with Calculations of Dimbylow and Mann

Even though all of our calculations have been done for plastic-covered handsets and antennas, we have made a limited number of runs using the same configurations as previously used by Dimbylow and Mann (1994). The objectives of these runs were to verify that the SAR distributions obtained at the European GSM frequencies of 900 MHz and 1800 MHz were fairly similar to those obtained by another research group which had used a very different model of the head and neck. For these test runs we used the tissue properties given in Table 5, which were taken from the paper as far as possible and likewise assumed the handset dimensions of 2.4 × 6 × 15 cm. Unlike the cubical cell sizes of 2 mm used by Dimbylow and Mann, we have taken a voxel size of 1.974 × 1.974 × 3 mm for our calculations. The summaries of the results obtained for the four test cases without the hand are given in Tables 6 and 7 for 900 and 1800

MHz, respectively. Also given as footnotes are the data calculated by Dimbylow and Mann for comparison. Since the exact weights of the 1 × 1 × 1 cm subvolume were not prescribed, we have considered the various subvolumes 1, 2, and 3 that were previously considered for the data given in Table 4. Also, even though the exact placements of the assumed handset vis-à-vis the ear were not exactly prescribed, it is interesting to note that the peak 1-gram SARs calculated for our model are fairly similar both at 900 and 1800 MHz. For our calculations we have assumed the feed points to be in the cross-sectional plane 6 mm below the top of the ear.

Tissue	Spec. Gravity 10^3kg/m^3	835 MHz		1900 MHz	
		ε_r	σ S/m	ε_r	σ S/m
muscle	1.04	58.00	1.21	56.00	1.76
fat	*0.92	*9.99	*0.17	*9.38	*0.26
bone (skull)	1.85	8.00	0.11	8.00	0.15
cartilage	1.10	35.00	0.60	32.00	0.57
skin	1.10	35.00	0.60	32.00	0.57
nerve	*1.04	*33.4	*0.60	*32.05	*0.90
blood	1.06	64.00	1.24	64.00	1.80
parotid gland	*1.05	*45.25	*0.92	*43.22	*1.29
CSF	1.06	72.00	2.13	72.00	2.50
eye humour	1.01	73.00	1.97	74.00	2.27
sclera	1.01	66.00	1.93	62.00	2.28
lens	1.05	44.00	0.80	42.00	1.19
pineal gland	*1.05	*45.26	*0.92	*43.22	*1.29
pituitary gland	*1.07	*45.26	*0.92	*43.22	*1.29
brain	1.03	49.00	1.10	47.00	1.42

* These values were not prescribed in Dimbylow and Mann (1994).

Table 5. Dielectric properties and specific gravities assumed for test runs for comparison with the calculations of Dimbylow and Mann (1994).

	No hand λ/4 antenna above handset	No hand λ/2 dipole
Peak 1-voxel SAR (W/kg)	7.57	9.13
Peak 1-g SAR (W/kg)[1]	2.07* (1.00 g; 92.0%)	2.10† (1.00 g; 92.0%)
Peak 1-g SAR (W/kg)[2]	2.49* (1.07 g; 83.0%)	2.71† (1.07 g; 83.0%)
Peak 1-g SAR (W/kg)[3]	2.45* (1.18 g; 86.1%)	2.47† (1.13 g; 81.5%)
Peak 1-g SAR for brain (W/kg)[2]	1.36 (1.01 g)	1.54 (1.01 g)
Peak 1-g SAR for brain (W/kg)[3]	1.31 (1.10 g)	1.48 (1.10 g)
Power absorbed by head and neck	51.7%	52.0%
Peak 1-voxel SAR for brain (W/kg)	4.6	2.6
CSF average (mW/kg)	62.3	60.7
Brain average (mW/kg)	74.4	88.0
Humour average (mW/kg)	50.6	42.8
Lens average (mW/kg)	26.5	19.8
Sclera average (mW/kg)	43.4	33.1

Superscripts 1, 2, and 3 are for cell numbers and subvolumes given in the footnote of Table 4.

* SAR scaled from Table 2 of Dimblyow and Mann (1994) = 2.17 W/kg.

† SAR scaled from Table 2 of Dimbylow and Mann (1994) = 2.02 W/kg.

Table 6. SAR distributions for the Utah model of the adult male without squished ear for comparison with data obtained by Dimbylow and Mann (1994) using the NRPB model. Frequency = 900 MHz. Radiated power = 600 mW. Distance of the source point to the ear = 1.38 cm (7 δ) as against 1.4 cm in Dimbylow and Mann (1994).

Effect of Tissue Properties on SAR Distributions

As given in Table 2, with both the old and the new values of dielectric properties, considerably higher values of ε_r and σ have recently been reported for fat, bone, and cartilage by C. Gabriel (1996). The ear is composed mainly of cartilage that is covered by the skin. In Table 3 we compare the salient features of the SAR distributions at 835 MHz that are obtained using both the new and old dielectric properties for these tissues. For this table and for Tables 8-10, we give the SARs that are calculated using the procedure suggested by the Dosimetry Working Group of WTR (see above).

Since some measurement systems for SAR evaluations use a homogeneous phantom model, also shown for comparison in Table 3 are the SARs obtained for the homogeneous model with properties identical to that of the brain at 835 MHz (see Table 2). It is interesting to note that the homogeneous model overestimates the peak 1-gram SAR by 42% as compared to that obtained using the anatomically based model. Use of homogeneous models could, therefore, lead to rejection of devices which would be considered in compliance with safety guidelines, had more realistic, anatomically-based models been used.

	No hand λ/4 antenna above handset	No hand λ/2 dipole
Peak 1-voxel SAR (W/kg)	1.54	1.90
Peak 1-g SAR (W/kg)[1]	0.53* (1.00 g; 98.7%)	0.55† (1.00 g; 98.7%)
Peak 1-g SAR (W/kg)[2]	0.87* (1.03 g; 80.0%)	0.81† (1.04 g; 81.0%)
Peak 1-g SAR (W/kg)[3]	0.83* (1.13 g; 81.5%)	0.76† (1.16 g; 83.3%)
Peak 1-g SAR for brain (W/kg)[2]	0.27 (1.04 g)	0.41 (1.01 g)
Peak 1-g SAR for brain (W/kg)[3]	0.27 (1.02 g)	0.40 (1.07 g)
Power absorbed by head and neck	45.4%	46.4%
Peak 1-voxel SAR for brain (W/kg)	0.50	0.64
CSF average (mW/kg)	7.8	9.0
Brain average (mW/kg)	10.4	13.2
Humour average (mW/kg)	8.8	7.4
Lens average (mW/kg)	2.5	2.0
Sclera average (mW/kg)	5.7	4.5

Superscripts 1, 2, and 3 are for cell numbers and subvolumes given in the footnote of Table 4.

* SAR scaled from Table 3 of Dimblyow and Mann (1994) = 0.70.

† SAR scaled from Table 3 of Dimbylow and Mann (1994) = 0.78.

Table 7. SAR distributions for the Utah model of the adult male without squished ear for comparison with data obtained by Dimbylow and Mann (1994) using the NRPB model. Frequency = 1800 MHz. Radiated power = 125 mW. Distance of the source point to the ear = 1.38 cm (7 δ) as against 1.4 cm in Dimbylow and Mann (1994).

	Adult male	10-year-old child	5-year-old child
Peak 1-voxel SAR (W/kg)	10.86	16.82	31.73
Peak 1-g SAR* (W/kg)	2.93 (1.00g)	3.21 (1.02 g)	4.49 (1.00 g)
Peak 1-g SAR for brain* (W/kg)	1.13 (1.09 g)	1.42 (1.00 g)	1.56 (1.00 g)
Power absorbed by head and neck	45.0%	42.6%	39.5%
Power absorbed by "hand"	9.2%	10.7%	5.5%
Peak 1-voxel SAR for brain (W/kg)	1.62	3.02	4.62
CSF average (mW/kg)	72.7	187.2	283.2
Brain average (mW/kg)	72.3	160.3	239.8
Humour average (mW/kg)	31.8	78.2	117.3
Lens average (mW/kg)	11.3	33.6	52.5
Sclera average (mW/kg)	17.8	48.7	73.7

* 5 x 5 x 4 cells; 0.987 x 0.987 x 1.200 cm; 1.170 cm^3 for the adult male
7 x 7 x 4 cells; 1.057 x 1.057 x 0.939 cm; 1.049 cm^3 for the 10-year-old child
8 x 8 x 5 cells; 1.039 x 1.039 x 0.950 cm; 1.026 cm^3 for the 5-year-old child

Table 8. Comparison of SAR distributions for models of an adult male and 10-year- and 5-year-old children. Frequency = 835 MHz. Time-averaged radiated power = 600 mW. A $\lambda/4$ antenna above a handset is taken for the calculations.

For each of the calculations given in Table 3, we have considered a quarter-wave monopole antenna above a handset of dimensions 2.96 × 5.73 × 15.5 cm (14 δ_x × 28 δ_y × 51 δ_z for the metal box covered with 1-mm-thick plastic on all sides) and the model of the adult male. The telephone is held against the left side of the head. The driving point of the monopole is located at the top of the handset, in the center of the 5.73 cm side furthest from the ear on the edge of the 2.96 cm side. The thin monopole antenna is assumed embedded in a covering sheath of dielectric material $\varepsilon_r = 4.0$ which, in the FD-TD formulation, is modeled by a 2 × 2 cell square stack of dielectric cells of cross-sectional dimensions 3.95 × 3.95 mm. New dielectric properties of the various tissues given in Table 2 are used for the results given in column 1 for these and all further cases considered in this paper.

Even though very similar fractional powers absorbed by the whole head are obtained for all three models, the peak 1-voxel SARs are considerably higher for the models using the newer higher conductivities for the cartilage (Table 2). Furthermore, the homogeneous model grossly overestimates the SAR and is also incapable of

providing tissue-relevant SAR distributions.

	Adult male	10-year-old child	5-year-old child
Peak 1-voxel SAR (W/kg)	3.90	4.9	6.20
Peak 1-g SAR* (W/kg)	1.11 (1.03 g)	0.90 (1.02 g)	0.97 (1.07 g)
Peak 1-g SAR for brain* (W/kg)	0.20 (1.00 g)	0.25 (1.07 g)	0.31 (1.00 g)
Power absorbed by head and neck	35.6%	34.4%	32.2%
Power absorbed by "hand"	13.8%	9.4%	6.8%
Peak 1-voxel SAR for brain (W/kg)	0.29	0.42	0.61
CSF average (mW/kg)	8.0	20.6	33.4
Brain average (mW/kg)	7.6	19.6	32.9
Humour average (mW/kg)	3.2	17.4	39.2
Lens average (mW/kg)	1.5	7.6	17.8
Sclera average (mW/kg)	1.8	9.9	20.5

* 5 x 5 x 4 cells; 0.987 x 0.987 x 1.200 cm; 1.170 cm^3 for the adult male
7 x 7 x 4 cells; 1.057 x 1.057 x 0.939 cm; 1.049 cm^3 for the 10-year-old child
8 x 8 x 5 cells; 1.039 x 1.039 x 0.950 cm; 1.026 cm^3 for the 5-year-old child

Table 9. Comparison of SAR distributions for models of an adult male and 10-year- and 5-year-old children. Frequency = 1900 MHz. Time-averaged radiated power = 125 mW. A $\lambda/4$ antenna above a handset is taken for the calculations.

Effect of Head Size on SAR Distributions: Comparison for Adult and 10- and 5-year-old Children

As previously described in the section regarding anatomic models of the human body, we have developed smaller models of the head, neck, and "hand" by reducing the voxel size 1.974 × 1.974 × 3.0 mm of the MRI-based model to new voxel sizes of 1.51 × 1.51 × 2.3469 mm and 1.2989 × 1.2989 × 1.9048 mm in order to obtain dimensions characteristic of 10- and 5-year-old children, respectively. In Tables 8 and 9, we give the salient features of the SAR distributions obtained for quarter-wave monopole antennas mounted as discussed earlier at irradiation frequencies of 835 and 1900 MHz, respectively. It is interesting to note that even though the peak 1-gram SARs are fairly similar for the three models at 1900 MHz, the 1-gram SARs are considerably higher

for the smaller head sizes at 835 MHz (Table 8). Also, the peak 1-voxel SARs are higher and a larger in-depth penetration of absorbed energy or higher SARs are obtained for the smaller models both at 835 and 1900 MHz. The fact that there is a larger in-depth penetration of SARs for the models of 10- and 5-year-old children as compared to those for the model of the adult is illustrated in Figures 8 and 9 for 835 and 1900 MHz, respectively. Because of a larger depth of penetration of EM fields at 835 MHz into the heads of the smaller subjects, increasing SARs are obtained for smaller models at this frequency. A similar trend of increasing 1-gram SARs for the smaller models at 835 MHz has also been observed for a longer 3 $\lambda/8$ antenna for which the SAR distributions are given in Table 10. The higher 1-voxel SARs for the smaller models in Table 8-10 are likely due to the thinner ears, which results in the antennas being somewhat closer to the region of highest SARs that are observed generally at the points of contact of the squished ear to the scalp of the head.

	Adult male	10-year-old child	5-year-old child
Peak 1-voxel SAR (W/kg)	5.97	7.65	12.75
Peak 1-g SAR* (W/kg)	1.60 (1.00 g)	1.49 (1.00 g)	1.88 (1.00 g)
Peak 1-g SAR for brain* (W/kg)	0.65 (1.05 g)	0.78 (1.00 g)	0.85 (1.00 g)
Power absorbed by head and neck	33.7%	28.8%	25.5%
Power absorbed by "hand"	5.6%	4.3%	2.8%
Peak 1-voxel SAR for brain (W/kg)	0.93	1.40	2.01
CSF average (mW/kg)	79.8	170.6	244.5
Brain average (mW/kg)	63.9	125.5	183.0
Humour average (mW/kg)	21.4	46.5	69.8
Lens average (mW/kg)	7.9	20.6	31.2
Sclera average (mW/kg)	12.0	29.3	43.3

* 5 x 5 x 4 cells; 0.987 x 0.987 x 1.200 cm; 1.170 cm^3 for the adult male
7 x 7 x 4 cells; 1.057 x 1.057 x 0.939 cm; 1.049 cm^3 for the 10-year-old child
8 x 8 x 5 cells; 1.039 x 1.039 x 0.950 cm; 1.026 cm^3 for the 5-year-old child

Table 10. Comparison of SAR distributions for models of an adult male and 10-year- and 5-year-old children. Frequency = 835 MHz. Time-averaged radiated power = 600 mW. A $3\lambda/8$ antenna above a handset is taken for the calculations.

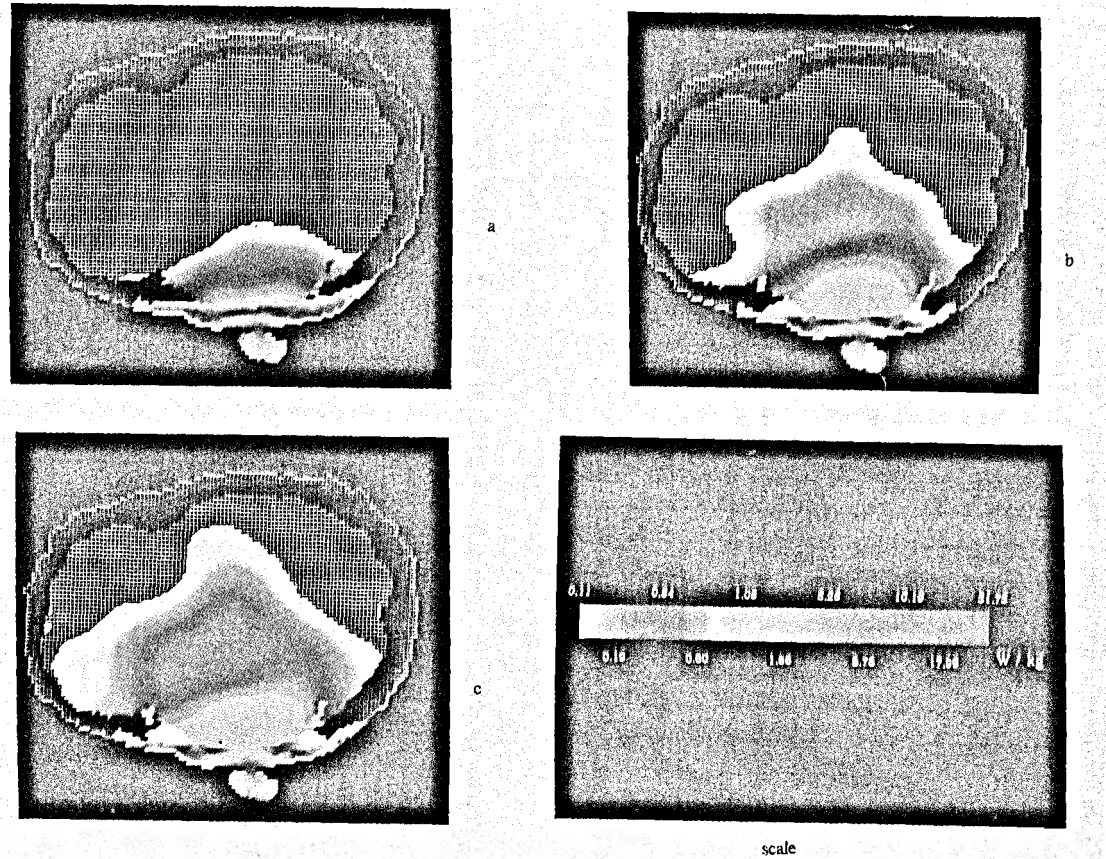

Figure 8. The SAR distribution for layer no. 34 models of an adult male and 10-year- and 5-year-old children (marked a, b, c). This layer contains the feed point and is two cells lower than the cross-sectional plane passing through the top of the ear for each of the models. Frequency = 835 MHz. Radiated power = 600 mW.

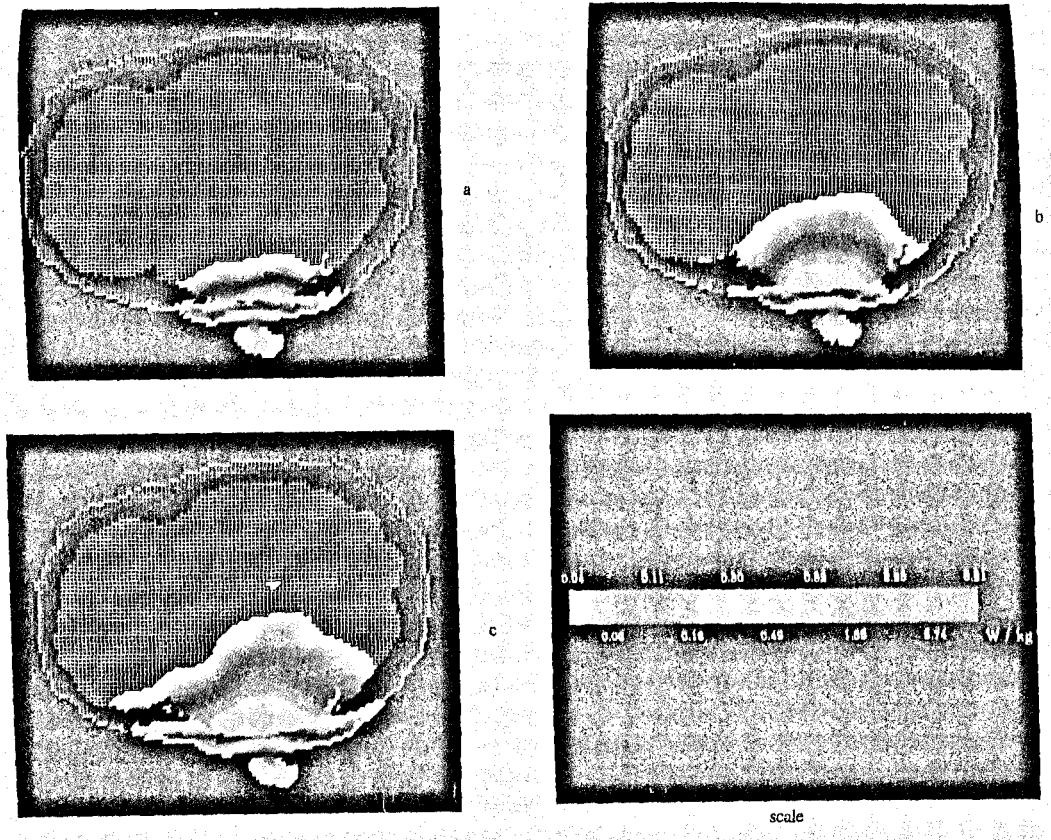

Figure 9. The SAR distribution for layer no. 34 for models of an adult male and 10-year- and 5-year-old children (marked a, b, c). This layer is two cells lower than the cross-sectional plane passing through the top of the ear for each of the models. Frequency = 1900 MHz. Radiated power = 125 mW.

Experimental Models

As previously mentioned in in the section on measurement methods, experimental methods have been used for over 25 years to obtain SAR distributions for far-field and near-field exposure conditions (Balzano et al., 1978, 1995; Bassen & Babij, 1990; Chatterjee et al., 1985; Chou, personal communication, 1994; Cleveland & Athey, 1989; Gabriel, personal communication, 1994; Gandhi & Chen, 1995; Gandhi et al., 1995; Guy & Chou, 1986; Johnson & Guy, 1972; Stuchly et al., 1986; Kuster & Balzano, 1992; Schmid et al., 1996; Stuchly & Stuchly, 1995). Tissue-simulant materials, both in the form of liquids and semi-solid gels (Chan, unpublished data; Cheung & Koopman, 1976; Chou, Chen, Guy, & Luk, 1984; Hartsgrove, Kraszewski, & Surowiec, 1987; Johnson & Guy, 1972) have been developed, the latter permitting tissue-dependent heterogeneous representation of the exposed models. For mobile telephone dosimetry, as shown in Table 3, use of homogeneous models can result in SARs that are considerably higher than those for heterogeneous, anatomically correct models. The lower peak 1-gram SARs for the anatomically based models are likely due to somewhat lower SARs for the cartilage-dominated region of the ear and the considerably smaller SARs for the relatively thick (approximately 1 cm), lower-conductivity region of the skull. For compliance testing, use of homogeneous models may result in rejection of devices which would be considered in compliance if heterogeneous thicker-skull models are used.

To provide realism for experimental modeling, several investigators, (e.g., Chou, personal communication, 1994; Cleveland and Athey, 1989; Gabriel, personal communication, 1994), have developed realistically shaped, heterogeneously-filled models that are filled with biological phantom materials simulant of tissues such as skull, brain, muscle, eyes, etc. All of these models use skull-shaped shells with substantial thicknesses that are representative of the human skull. Even though these models do not have the anatomical details such as are possible with computer-based numerical procedures, they are a considerable improvement over homogeneous models in not increasing the SARs artificially. Simplicity of the model and convenience in its use have often been cited as the reasons for using homogeneous models for compliance testing of mobile telephones. It is claimed that for certain types of antennas, the overestimation of the spatial-peak SAR averaged over 1 gram is within 33% of the values obtained using anatomically correct models (Hombach et al., 1996; Kuster 1998). But this last statement cannot be considered to be based on any rigorous scientific arguments. Indeed, the overestimation provided by the homogeneous model may vary with frequency and the nature of the antenna and the handset. Since compliance testing of mobile telephones being introduced into society is an important issue and millions of each type of telephone are likely to be used by consumers, it makes no sense to take shortcuts by using homogeneous experimental models when heterogeneous models are available and are being increasingly used for such testing.

Concluding Remarks

Since it is a near-field problem, both the calculations and the measurements of SAR distributions are sensitive to the placement of the source vis-à-vis the body and the models that are used. Small differences in the reported SAR distributions are, therefore, likely due to both of these issues. Compliance testing is much easier if a given device results in peak 1-gram or 10-gram SARs that are well within the safety guidelines (ANSI/IEEE, 1992; CENELEC, 1995). The problem is considerably harder for devices for which the SARs are close to the limits of the safety guidelines. In the absence of testing procedures defined by the consensus standard-setting groups such as ANSI/IEEE, expert groups such as the Dosimetry Working Group of WTR and others need to define procedures that may be used for compliance testing of wireless communication devices.

Acknowledgments

The author gratefully acknowledges the contributions of his colleagues, Gianluca Lazzi and Cynthia M. Furse, to this work. The validation test runs described were done by Cynthia Furse (Furse & Gandhi, 1995), while the data given in Tables 3-10 was obtained by Gianluca Lazzi. The graphics for Figures 7-9 were done by Vishram Pandit.

Notes

[1] The effective dielectric constant ε_{eff} is derived by noting that the dielectric fields close to the metallic surface such as that of a handset are primarily normal, and only a part of the FD-TD cell width is actually filled with the dielectric material. The required continuity of the normal component of $D = \varepsilon E$ with outer region can be used to obtain ε_{eff}.

[2] Dosimetry Working Group of WTR consists of the following individuals: A. W. Guy (Chairman), C. K. Chou, C. Gabriel, O. P. Gandhi, N. Kuster, R. Petersen, P. Polson, V. Santomaa, Q. Balzano, and A. Taflove.

References

American National Standards Institute/Institute of Electrical and Electronics Engineers (ANSI/IEEE). (1992). Standard for safety levels with respect to human exposure to radio frequency electromagnetic fields, 3 kHz to 300 GHz (Rep. C95.1-1992). New York: Institute of Electrical and Electronics Engineers, Inc.

Balzano, Q., Garay, O., & Steel, F. R. (1978). Energy deposition in simulated human operators of 800-MHz portable transmitters. IEEE Transactions on Vehicular Technology, 27(4), 174-181.

Balzano, Q., Garay, O., & Manning, T. (1995). Electromagnetic energy exposure of simulated

users of portable cellular telephones. IEEE Transactions on Vehicular Technology, 44, 390-403.

Bassen, H. I., & Babij, T. M. (1990). Experimental techniques and instrumentation. In O. P. Gandhi (Ed.), Biological effects and medical applications of electromagnetic energy (pp. 141-173). Englewood Cliffs, NJ: Prentice Hall.

Bassen, H. I., & Smith, G. S. (1983). Electric field probes: A review. IEEE Transactions on Antennas and Propagation, 31(5), 710-718.

Berenger, J. P. (1994). A perfect matched layer for the absorption of electromagnetic waves. Journal of Computational Physics, 114, 185-200.

Berntsen, S., & Hornsleth, S. N. (1994). Retarded time absorbing boundary conditions. IEEE Transactions on Antennas and Propagation, 42, 1059-1064.

CENELEC European Prestandard ENV 50166-2, (1995). Human Exposure to Electromagnetic Fields: High Frequency (10 kHz to 300 GHz). CENELEC Central Secretariat: rue de Stassart 35, B-1050, Brussels, Belgium.

Chan, K.W. Microwave phantoms. Unpublished report.

Chatterjee, I., Gu, Y. G., & Gandhi, O. P. (1985). Quantification of electromagnetic absorption in humans from body-mounted communication transceivers. IEEE Transactions on Vehicular Technology, 34(1), 55-62.

Cheung, A. Y., & Koopman, D. W. (1976). Experimental development of simulated biomaterials for dosimetry studies of hazardous microwave radiation. IEEE Transactions on Microwave Theory and Technique, 24, 669.

Chou, C. K., Chen, G. W., Guy, A. W., & Luk, K. H. (1984). Formulas for preparing phantom muscle tissue at various radiofrequencies. Bioelectromagnetics, 5, 435-441.

Cleveland, R. F., & Athey, T. W. (1989). Specific sbsorption rate (SAR) in models of the human head exposed to handheld UHF portable radios. Bioelectromagnetics, 10(2), 173-186.

CST. (1994). The MAFIA Collaboration. User's Guide Mafia Version 3.x. Darmstadt, Germany: CST GmbH.

Cui, Y., Chen, J. Y., & Gandhi, O. P. (1995, June). Comparison of various boundary conditions for SARs and radiation patterns of cellular telephones [abstract]. In The seventeenth annual meeting of the Bioelectromagnetics Society, Boston, Massachusetts abstract book, 31.

Dhondt, G. & Martens, L. (1994, November). A canonical case with an analytical solution for the comparison of electromagnetic field solvers. In D. Simunic (Ed.), Proceedings of the COST 244 Meeting on Reference Models for Bioelectromagnetic Test of Mobile Communication Systems, Rome, Italy, 98-104.

Dimbylow, P. J., & Mann, S. M. (1994). SAR calculations in an anatomically based realistic model of the head for mobile transceivers at 900 MHz and 1.8 GHz. Physics in Medicine and Biology, 39, 1537-1553.

Durney, C. H., Massoudi, H., & Iskander, M. F. (1986). Radiofrequency radiation dosimetry

handbook (4th ed., Rep. No. USAF SAM-TR-85-73). Brooks Air Force Base, TX: USAF School of Aerospace Medicine, Aerospace Medical Division.

Federal Communications Commission. (1994, June). Amendment of the Commission's rules to establish new personal services (No. FCC, 94-144). Washington, DC: Federal Communications Commission.

Furse, C. M., & Gandhi, O. P. (1995, October). Validation of the FDTD method for canonical problems with near-field sources (Interim Report No. 1). Submitted to Wireless Technology Research, LLC, Washington, D.C.

Gabriel, C. (1996). Compilation of the Dielectric Properties of Body Tissues at RF and Microwave Frequencies (AL/OE-TR 1996-0037). Brooks Air Force Base, TX: Occupational and Environmental Health Directorate, Radiofrequency Radiation Division.

Gandhi, O. P. (1990). Numerical methods for specific absorption rate calculations. In O. P. Gandhi (Ed.), Biological effects and medical applications of electromagnetic energy (pp. 113-140). Englewood Cliffs, NJ: Prentice Hall.

Gandhi, O. P. (1995). Some numerical methods for dosimetry: Extremely low frequencies to microwave frequencies. Radio Science, 30, 161-177.

Gandhi, O. P., & Chen, J. Y. (1995). Electromagnetic absorption in the human head from experimental 6-GHz handheld transceivers. IEEE Transactions on Electromagnetic Compatibility, 37, 547-558.

Gandhi, O. P., Chen, J. Y., & Wu, D. (1994, September). Electromagnetic absorption in the human head for mobile telephones at 835 and 1900 MHz. In Proceedings of the International Symposium on Electromagnetic Compatibility EMC '94, Rome, Italy, 1-5.

Gandhi, O. P., Gu, Y. G., Chen, J. Y., & Bassen, H. I. (1992). SAR and induced current distributions in a high-resolution anatomically based model of a human for plane-wave exposures 100-915 MHz. Health Physics, 63, 281-290.

Gandhi, O. P., Sedigh, K., Beck, G. S., & Hunt, E. L. (1976). Distribution of electromagnetic energy deposition in models of man with frequencies near resonance. In Biological effects of electromagnetic waves (Publication No. 77-8011, pp. 44-67). Rockville, MD: Bureau of Radiological Health, Food and Drug Administration, U. S. Department of Health, Education and Welfare.

Guy, A. W., & Chou, C. K. (1986). Specific absorption rate of energy in man models exposed to cellular UHF mobile antenna fields. IEEE Transactions on Microwave Theory and Technique, 34(6), 671-680.

Hartsgrove, G., Kraszewski, A., & Surowiec, A. (1987). Simulated biological materials for electromagnetic radiation absorption studies. Bioelectromagnetics, 8, 29-36.

Hombach, V., Meier, K., Burkhardt, M., Tay, R., & Kuster, N. (1996). The dependence of EM energy absorption upon human head modeling at 1800 MHz. IEEE Transactions on Microwave Theory and Technique, 44, 1865-1873.

International Council on Radiation Protection (ICRP). (1992). Report of the task group on

reference man (Rep. No. 23). New York: Pergamon Press.

Jensen, M. A., & Rahmat-Samii, Y. (1995). EM interaction of handset antennas and a human in personal communications. Proceedings of the IEEE, 83, 7-17.

Johnson, C. C., & Guy, A. W. (1972). Nonionizing electromagnetic wave effects in biological materials and systems. Proceedings of the IEEE, 60, 692-718.

King, R. W. P. (1993). The electromagnetic field of a horizontal electric dipole in the presence of a three-layered region: Supplement. Journal of Applied Physics, 74, 4845-4848.

Kunz, K. S., & Luebbers, R. J. (1993). The finite-difference time-domain method in electromagnetics. Boca Raton, FL: CRC Press.

Kuster, N. (1998). Compliance testing of handheld mobile communications equipment. In G. L. Carlo (Ed.), Wireless phones and health: Scientific progress (pp. 47-54). Norwell, MA: Kluwer Academic Press.

Kuster, N., & Balzano, Q. (1992). Energy absorption mechanism by biological bodies in the near field of dipole antennas above 300 MHz. IEEE Transactions on Vehicular Technology, 41(1), 17-23.

Lazzi, G., & Gandhi, O. P. (1997). Realistically tilted and truncated anatomically based models of the human head for dosimetry of mobile telephones. IEEE Transactions on Electromagnetic Compatibility, 39(1), 55-61.

Lentner, C. (Ed.). (1984). Geigy scientific tables. Basle, Switzerland: CIBA-GEIGY Limited.

Lin, J. C., & Gandhi, O. P. (1995). Computational methods for predicting field intensity. In C. Polk & E. Postow (Eds.), Handbook of biological effects of electromagnetic fields (pp. 337-402). Boca Raton, FL: CRC Press.

Mur, G. (1981). Absorbing boundary conditions for the finite-difference approximation of the time-domain electromagnetic-field equations. IEEE Transactions on Electromagnetic Compatibility, 23, 337-382.

Schmid, T., Egger, O., & Kuster, N. (1996), Automated E-field scanning systems for dosimetric assessments. IEEE Transactions on Microwave Theory and Technique, 44 (1), 105-113.

Simunic, D. (Ed.). (1994, November). Reference models for bioelectromagnetic test of mobile communication systems. Proceedings of the COST 244 Meeting, Rome, Italy.

Stuchly, M. A., Spiegel, R. J., Stuchly, S. S., & Kraszewski, A. (1986). Exposure of man in the near field of a resonant dipole: Comparison between theory and measurements. IEEE Transactions on Microwave Theory and Techniques, 34, 26-31.

Stuchly, M. A., & Stuchly, S. S. (1995). Experimental radio and microwave dosimetry. In C. Polk & E. Postow (Eds.), Handbook of biological effects of electromagnetic fields (2nd ed., pp. 295-336). Boca Raton, FL: CRC Press, Inc.

Stuchly, M. A., & Stuchly, S. S. (1980). Dielectric properties of biological substances -- Tabulated. Journal of Microwave Power, 15, 19-26.

Taflove, A. (1995). Computational electrodynamics: The finite-difference time-domain method. Dedham, MA: Artech House.